POLITECNICO
MILANO 1863

SCUOLA DI INGEGNERIA INDUSTRIALE
E DELL'INFORMAZIONE

Executive Summary of the Thesis

Wind tunnel testing of propeller interaction for a novel push-pull aircraft configuration

Laurea Magistrale in Aeronautical Engineering - Ingegneria Aeronautica

Author: Elisa G. Garbin, R. Andrew Oggioni

Advisor: Prof. Maurizio Boffadossi

Co-advisor: Prof. Carlo E. D. Riboldi

Academic year: 2022-2023

1. Introduction

The aim of this Master's Thesis is to verify and conduct an in-depth study of the turbo-prop aircraft M.E.L.S.A. Kestrel propulsive solution. The conceptual design of this aircraft was conducted during the academic course of "Progetto di Velivoli" with the help of the Italian Air Force, and features peculiar characteristics like the push-pull in-tandem propellers configuration and a triple tail.

Figure 1: The Kestrel

The literature exploring these specific solutions is not exhaustive, mainly because investigations in this field were abandoned with the advent of jet engines. Therefore, the desire to better understand the implications related to the Kestrel peculiar aspects, led to the decision to create a re-scaled model for conducting tests from various perspectives: propulsive and aeromechanical point of view. These two fields consistently showcased their interconnectedness throughout the analysis.

The propulsive aspect is studied as both a phenomenon and a mean to generate crucial results for advancing the sizing and design of the re-scaled radio-controlled (R/C) flying model.

To delve into the propulsive solution, measuring the thrust obtained coupling the motor and propeller, and estimating effects related to the in-tandem position, the authors initiated with a preliminary extensometric gauge. Subsequently, a more comprehensive analysis unfolded in the "De Ponte" wind tunnel, considering the influence of wind speed. It allowed to construct Penaud diagrams, instrumental for the performance study.

The flight model had to be estimated to assess the airworthiness of the re-scaled aircraft. It involved computing control and stability derivatives and airplane modes to establish a preliminary flight model. This step was conducted analytically following Roskam,[5] and Torenbeek, [6] and then compared to the numerical results

obtained with `OpenVSP`. Subsequently, a comprehensive plan was formulated for a flight test campaign to validate this preliminary model, utilizing the constructed R/C aircraft.

2. The Kestrel

The Kestrel is an aircraft designed for Close Air Support (CAS) missions and COunterINsurgency (COIN) operations against paramilitary or guerrilla organizations. The Kestrel features a rare propulsive solution known as push-pull.
The push-pull configuration, in particular, offers several advantages from both a piloting and performance perspective. With the motors in tandem, they are aligned along the rolling axis, ensuring they do not influence the inertia on this axis, thereby providing a quicker rolling time. This quality is further complemented by easier piloting, with a reduced workload, in the event of an OEI (One Engine Inoperative) condition, as the plane's behavior remains symmetric.
From an aerodynamic perspective, when compared to a traditional twin engine, it offers a reduced frontal section and, consequently, reduced drag. Despite having the same power, this configuration results in better performance and lower consumption.

Empty weight	3550 kg
MTOW	6500 kg
Wing span	14.42 m
Wing area	28.87 m^2
Payload	2000 kg
Engine power	670 kW
Combact range	425 km

Table 1: Kestrel characteristics and performance

3. The design of the R/C model

The 1:7 scaled model was designed to maintain the overall shape of the original Kestrel. The wingspan obtained is 2.07 m, while the length is of 1.3 m. A change in the Reynolds regime, in comparison with the original aircraft, had to be taken into account. The Kestrel has a Mean Aerodynamic Chord (MAC) of 0.28 m, representing the characteristic length of the model, and the typical flying speed preliminary estimated to be around 23.3 m/s (84 km/h). Consequently, it is possible to compute the actual Reynolds number:

$$Re = \frac{MAC\ V}{\nu} = 460000 \tag{1}$$

Where $\nu = 1.42e^{-5}\ m^2/s$ is the kinematic viscosity at 10°. These considerations are important as the coefficients, describing the performance of an airfoil, are heavily influenced by the Reynolds number. Following this reason, it is necessary to replace the original airfoil with a new one. The Clark Y airfoil is selected after a comparison with other airfoils using tabulated data available in bibliography, [1], and using panel-based methods, like `XFLR5`. Other aspects that have been altered from the original plane include the wing and tail incidence, as well as the removal of the twist along the wingspan. It was necessary to define all the required components inside the fuselage to properly conduct the weight (5.5 kg) and balance of the aircraft and place the center of mass with precision. This information is crucial in stability calculations.

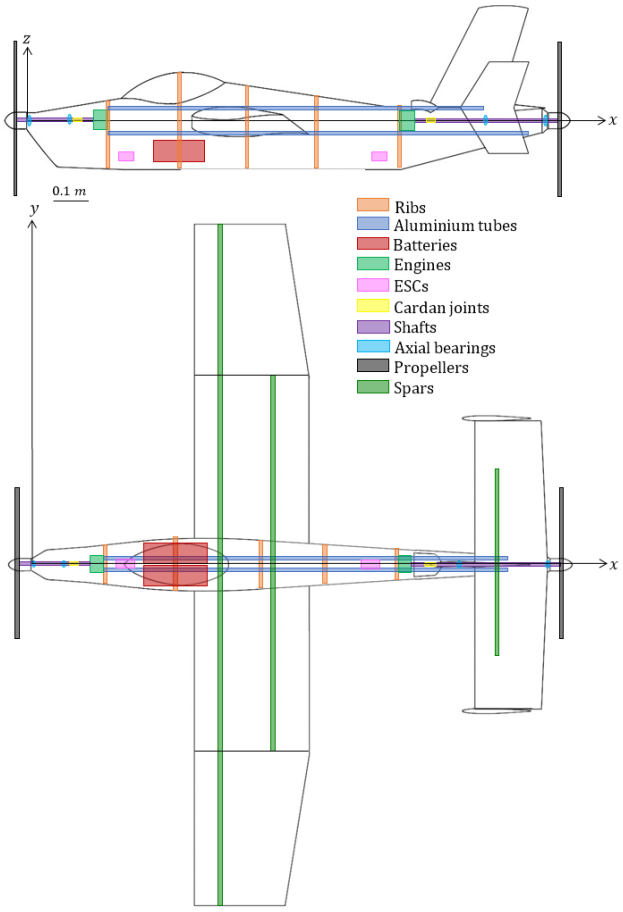

Figure 2: Kestrel internal lofting

With the redesigned wing and the center of mass

defined, the following step is to verify the static and dynamic stability of the aircraft through the computation of stability derivatives. This is achieved using both an analytical method, following Roskam's suggestions, [5], and implementing a numerical model after building the Kestrel in `OpenVSP`. The results closely match.
It is important to underline that during this phase, an estimation of the total drag coefficient was computed with `VSPAERO`, using Torenbeek equations, [6].

4. Building the model

Before beginning the design process of the R/C model, a research regarding the state of the art of the radio modelling was conducted, focusing on the building techniques and acquiring all the competence to realize the components inside a remote model. To conduct this activity a twin-engine B25 Mitchell, with a wingspan of 1.74 m was built and maiden flight. This specific model was chosen for its overall shape similarity and the innovative approach to constructing the internal structure through the implementation of 3D printing.
The 1:7 scaled model is designed using `Autodesk®` `Inventor®` and produced mainly with an FDM 3D printing method with PLA material. This building technique guarantees easy production of the parts and quick repair.
The design phase is divided into three main groups: fuselage and internal structure, wings, and tails. Here, for the sake of brevity, the main challenges faced during the design of each crucial components are reported.

4.1. Fuselage

As the fuselage is composed by seven thin shells, loading it with the weight and forces from the propulsive components is not viable due to the potential risk of layer separation or segment detachment. To achieve it, a bending-resistant structure is created using four aluminum tubes, preventing instability effects and connecting fuselage segments. Ribs are then introduced to link the outer shell with the inner tubes and transfer externally acting loads to the internal structure.

4.2. Wing and tail surfaces

Realizing the wing, it was necessary to create the external shape with the Clark Y airfoil. Internally, a lattice structure had to be constructed to provide stiffness while remaining light and easy to print. In the same way the tail surfaces are designed. This structure recalls the geodetic structure.

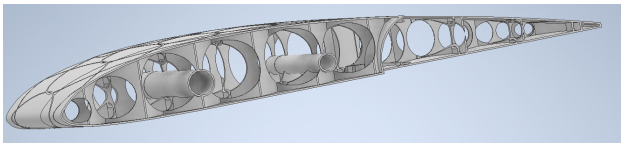

Figure 3: Internal structure of the wing

4.3. Landing gear

The landing gear represented another challenge due to the loads it had to face, with the objective of creating a lightweight component. For this reason, the decision was made to build it in carbon fiber instead of aluminum, aiming to reduce weight and ensure sufficient stiffness.

4.4. Propeller shaft

Due to lofting reasons, both motors are placed far apart from the respective propellers, necessitating the installation of two shafts connecting them. The fabrication of the propeller shafts posed a significant challenge during the process. One of the associated issues involved establishing a secure connection between the shaft and the pin from the `AXI motor`, especially considering potential minor misalignments upon insertion into the nose or rear structure. Addressing this concern necessitated the selection of a joint which could offer flexibility to accommodate misalignments during rotation while simultaneously withstanding the torque imposed by the motor during spinning, stopping, or starting. Moreover, the shaft was produced in carbon fiber with the aim of introducing a structural breaker to protect the motor in case of impact. The shaft is kept in place by ball-bearings.

4.5. Validation of the air-frame

The designed structure was validated in two separate phases. The fuselage structure was assessed during the gauge tests, being loaded with the forces generated by the motors and working propellers, while the wings underwent a more detailed examination. The bending of the wing was considered the main risk of breakage due to the nature of the printed parts and the alignment of the layers. For this reason a static struc-

tural test of the wing was conducted.
Starting from the VLM prediction of the lift distribution, loads are computed and transformed into sandbags. They are then symmetrically displaced along the inverted wing to recreate the loads up to 4 g, which is the maximum load factor obtained from the $V-n$ diagram estimated with Roskam, [5]. A maximum deflection of 10 cm was achieved.

5. Static thrust measurement

The experimental activity began with gauge implementation, aiming to provide an initial estimation of the thrust generated by the coupling of the propeller and the motor and initiating a study on propeller interaction.

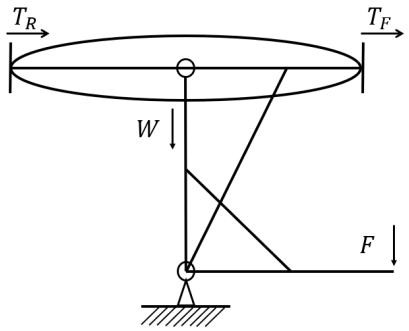

Figure 4: Static thrust measurements test bed

$$F = T_F + T_R$$

This method was validated with a comparison of the data obtained by `APC® propellers`.

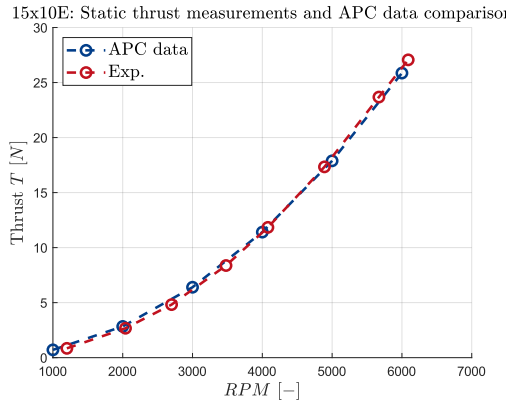

Figure 5: Static thrust measurements compared to `APC® propellers`

The design outcome was the selection of the propellers, the `Master Airscrew®` three-bladed 16"x10", tractor for front and pusher for the rear, which best suited the needs of the test, generating enough thrust to guarantee also the OEI condition during the flight campaign.

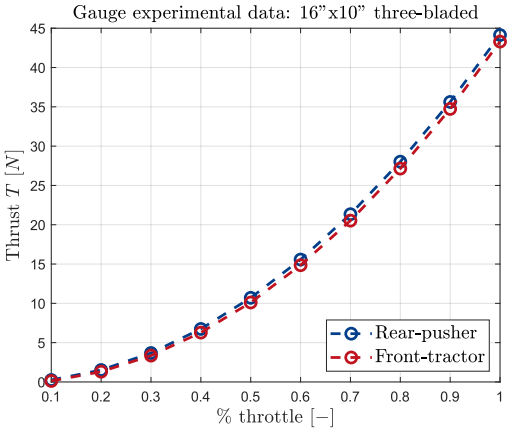

Figure 6: Front and rear propeller static thrust measurements comparison

One of the main findings indicates that, from the recorded data, it is evident that the rear propeller, both when operating alone and when implemented on the fuselage, can produce greater thrust compared to the front propeller at the same RPM. This result contradicts the initial expectation, where it was believed that the rear propeller would experience a less favorable working regime.

A possible explanation for this result arises when comparing the inflow and outflow conditions of the two propellers: the inflow condition impacts the performance less in comparison to the outflow. Specifically, the front propeller experiences outflow obstruction due to the presence of the fuselage, while the rear propeller can develop its wake without blocking effects.

The obtained data are then used to numerically estimate the variation of thrust with wind speed, defining a preliminary Penaud diagram. It is useful in determining the speeds achievable by the model and guiding the sizing during the design process. These results are later compared with the wind tunnel data, fig. 7.

6. Wind tunnel test

The primary objective of the wind tunnel campaign is to characterize the propulsion system in the push-pull configuration, with a particular focus on the interaction between the wake generated by the front propeller and the operating regime of the rear disk. Being the thrust

heavily influenced by the speed of the incoming flow, tests are done for six values of speed: 0 m/s, 10 m/s, 12.5 m/s, 15 m/s, 17.5 m/s and 20 m/s.
The activity is conducted in the "De Ponte" wind tunnel, capable of reaching speeds up to 56 m/s with a maximum power of 100 kW, featuring also a pressure compensation system. The test chamber dimensions are 1 m wide, 1.5 m high and 3m long. The model is positioned with an angle of attack of 0° to replicate the cruise condition.

6.1. Wind tunnel test bed

In the wind tunnel test, the necessity of installing a load cell to measure force through its own deformation introduces the requirement to minimize other structural deformations, ensuring a rigid transmission of loads through the structure to maintain the quality of measurements. For these reasons, the wind tunnel model must prioritize rigidity over weight. Following this principle, a new model was designed with stiffness as the top priority. The load-cell installed is a 535QD with a range of 0-12 kg, with a sensibility of 2 mv/V and an error of ± 0.023 over the full scale.

6.2. Propulsive characterization

The OEI_R condition produces more thrust than the OEI_F one, and it holds true for all speed and RPM ranges.

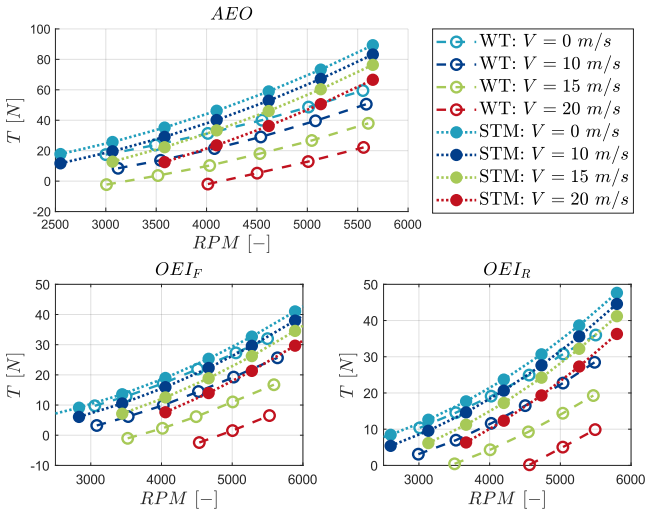

Figure 7: Wind tunnel and static thrust measurements comparison

The result is coherent with what emerged during the gauge tests. These data are also compared with the preliminary estimation of the change with the wind speed. It becomes evident that these estimations were too optimistic when compared to the real data. To define the goodness of these results, dimensionless transformation has done in fig. 8 using the advance ratio J and the thrust coefficient c_T, defined as:

$$J = \frac{V}{n_P\ D_P} \qquad c_T = \frac{T}{\rho\ n_P^2\ D_P^4} \tag{2}$$

With $n_P = RPM/60$, the rotation speed in $1/s$.

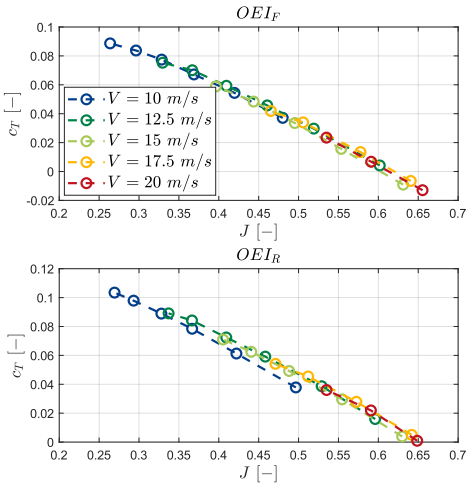

Figure 8: Advance coefficient J-thrust coefficient c_T

The following observations pertain to a comparison between the OEI and AEO regimes by varying the wind speed. The OEI values are summed up with respect to the AEO curve.

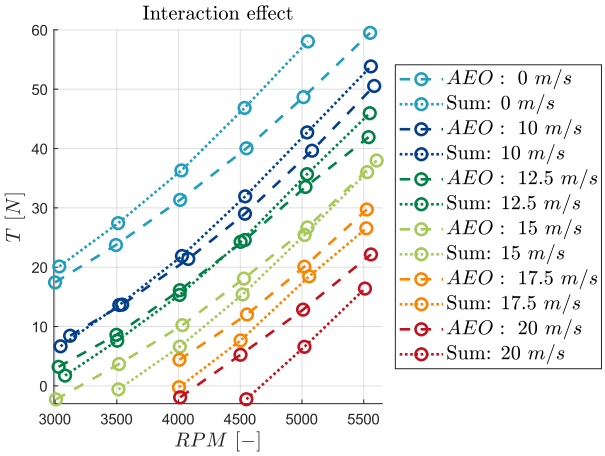

Figure 9: Interaction effects

At lower speeds, the algebraic sum surpasses the corresponding AEO value at each RPM.

This result was also noticeable during the fixed-point analysis conducted with the gauge. Instead, it becomes evident that there is a shift in behaviour while increasing the speed: the AEO condition develops more thrust with respect to the mere sum of the OEIs. Another intriguing observation lies in the difference in slope between AEO and the cumulative sum; indeed, the first one tends to favor lower values of RPM. It indicates that relying solely on a fixed-point analysis of the gauge would result in missing the correct trend when wind speed is different from zero, thereby misunderstanding the actual behavior of this propulsion solution. There are several hypotheses why this is happening: a first hypothesis is that the propellers are counter rotating. The rear propeller may encounter a wake which alters the speed triangles changing the flow speed, resulting in a different load on the rear disk. Another hypothesis is that the airflow around the fuselage, when the front propeller is operational, differs from the airflow without the propeller wake. The variation leads to a reduced flow velocity along the fuselage, consequently impacting the regime of the rear propeller, [2].
In fig. 9 it is evident that, with wind speeds exceeding 15 m/s, indicative of a cruise phase, the interaction exhibits a positive effect. Conversely, during low-speed maneuvers such as landing, with stall speed of 11 m/s, the interaction manifests a negative impact.

6.3. Performance

Following the new data, it is then possible to obtain a new Penaud diagram which better represents the actual performance.

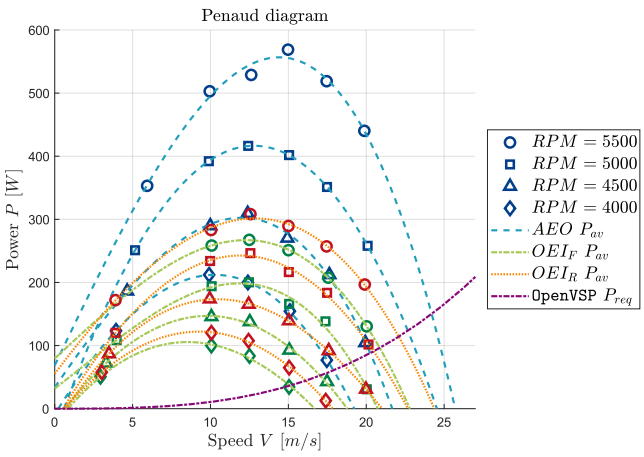

Figure 10: Wind tunnel Penaud diagram

The $P - V$ diagram confirms several observations already discussed in the comparison between OEI front and rear scenarios. In addition, it is possible to compare the required power P_{req} with the wind tunnel experimentally measured available power P_{av} while varying the RPM regime, representing the throttle, and the speed of flight. The P_{req} is estimated starting from the C_{D_0} obtained in `OpenVSP`.
It is feasible to determine the maximum speed for distinct propulsive configurations, with a peak speed of 24 m/s for the AEO, 22 m/s for OEI_R, and 21 m/s for OEI_F.

6.4. Tail effect

Among the tests conducted in the wind tunnel, an additional variable is introduced to the investigation. Specifically, the variation of the tail configuration is implemented to assess how the tail geometry can influence the operating regime of the rear propeller, [3]. Two tail configurations are implemented for comparison with the sole fuselage configuration: firstly, a segment of the horizontal tail alone, and subsequently, a segment of the horizontal tail with the addition of the central vertical tail. In analyzing the results, only OEI_R graphic is shown because the effect is more visible than AEO condition, where the front propeller, not affected by tail configuration reduce the visibility of the effect.

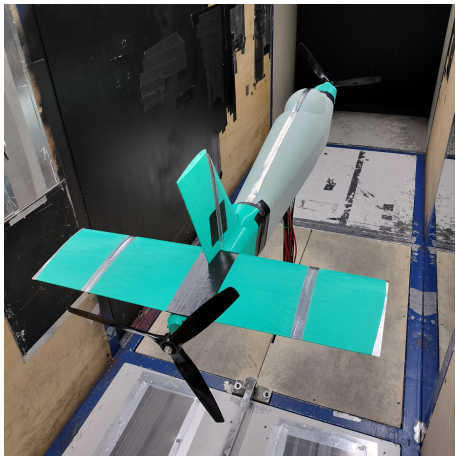

Figure 11: Wind tunnel model with tails

To provide a comprehensive commentary on these results, an error bar was introduced. It was based on a series of repetitions conducted during the test to analyze the repeatability of the results. This step was taken to ensure that any deviations from the baseline trend were not at-

tributed to measurement errors but rather indicative of actual phenomena at play.

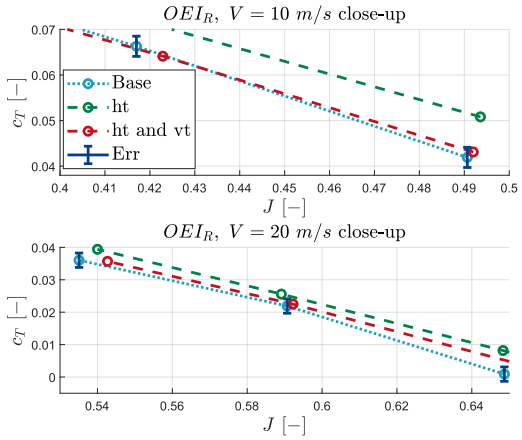

Figure 12: Comparison with different tail configuration RPM-thrust, OEI_R condition: Close-up

In the OEI_R condition, as evident in the dimensionless plot, fig. 12, there is a tendency in increasing thrust when only the horizontal tail configuration is employed. However, this advantageous gain achieved with the horizontal tail alone is subsequently diminished with the addition of the central vertical tail.
An interpretation of this phenomenon was considered: the horizontal surface is in close proximity to the propeller. This short distance allows limited time for the wake to develop vortices before being ingested by the propeller, thereby reducing the portion of the disk affected by the wake. Additionally, the horizontal surface may act as a stator, enhancing the flow coming from the fuselage.
In contrast, the central vertical tail begins approximately 10 cm before the horizontal tail and concludes earlier, leaving more space ahead of the rear propeller. Building upon the considerations made for the horizontal tail, the additional space allows more time for the wake to develop from the vertical surface and interact with a larger portion of the rear propeller. This effect could be further enhanced by the sweep introduced by the vertical tail.

6.5. Optimum throttle analysis

Another series of tests is conducted with an acquisition time of 100 s, recording propulsive sweeps. Each of the six studies is carried out in the AEO condition, maintaining a constant RPM value for one motor, while the RPM of the other motor is varied from 3000 to 5500 RPM with linear stepped increments. For the motor with constant RPM, three different values are explored: 3000, 4000, and 5000 RPM.

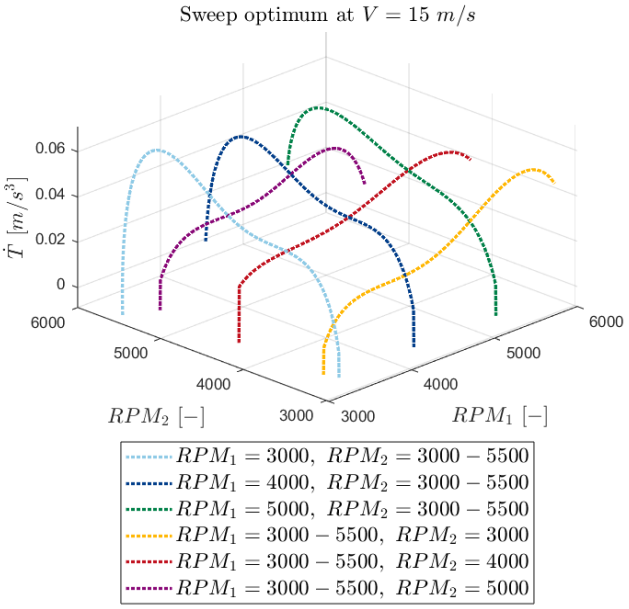

Figure 13: Thrust derivative as function of time for the six sweeps

The analysis is designed to ascertain whether an optimum throttle condition exists for each motor when the other one is fixed at certain values. It is conducted at 15 m/s to mitigate the risk of encountering negative values of thrust. The optimum study is realized based on the first derivative of the thrust as function of time. The resulting observation is interesting: although the fixed motor is set at three different RPM values, when it is the rear motor that is varying, it consistently reaches its optimum throttle at approximately $\sim$ 90%, whereas when the method is applied to the front motor while keeping the rear constant, it has its optimum operating point at around $\sim$ 92.5%. This observation leads in the definition of optimum operational conditions motors very useful, in the cruise flight phase.

7. Future development and flight test campaign

The aim of the thesis was to create a radio-controlled model of the Kestrel able to carry out a flight campaign. The aircraft model, along with its electronic configuration, has been completed. However, the flight campaign itself has not been conducted by the incoming deadline.
Using the Pixhawk PX4 the aim is to record fly-

ing data: then, the data can be compared with the preliminary flight model. This comparison is essential as it allows the verification of numerically estimated values. Moreover, given the absence of analytical equations in the literature perfectly fitting these geometries, refining stability and control derivatives becomes crucial for improving the available equations.
Subsequently, as the available power is estimated during the wind tunnel activity and having the capability to record the true airspeed (TAS) with an onboard Pitot tube, it becomes possible to estimate the actual drag coefficient of the plane. The flight campaign has been organized and programmed with a test matrix.

Furthermore, a new, more in depth and prolonged wind tunnel campaign can be conducted. The number of load cells can be increased from one to three, adding two more to the one that evaluates the total longitudinal force, one for each motor to provide partial values. This configuration enables an in depth analysis of the propellers' interaction. Furthermore, in the comprehensive interaction study, a portion of the wing can be added, working within a larger test chamber. Additionally, implementing tail control surfaces enables the analysis of how the rear propeller's working regime is altered when deflecting the control surface. Simultaneously, there could be a related study of improvements in the reactance of the controls due to the flow aspirated by the rear propeller.

Further improvements in the future can be achieved through the use of a numerical predictive method, such as a specialized program for rotors, like DUST.

8. Conclusions

This study paves the way for a more in-depth exploration of the push-pull configuration, with a specific focus on the interaction established between the two counter rotating, tandem propellers. From a propulsive standpoint, what is evident is that the interaction becomes positive beyond a certain wind speed, providing superior thrust compared to the sum of each motor nominal one. In particular, an unexpected result has been discovered: the rear propeller, when rotating at the same RPM regime as the front propeller, is capable of generating higher thrust. This phenomenon is believed to be linked to the different outflow conditions. In the case of the front propeller, the outflow is obstructed by the fuselage, thereby reducing the front motor's performance. This observation also suggests that the inflow condition, in this configuration, has a lesser impact than the outflow condition on a propeller disk. From a flight mechanics perspective the rear propeller has a stabilizing effect, hence the outperforming of that, it is particularly interesting, [4]. Furthermore, the interaction with both the horizontal and vertical tail suggests a varying effect based on the distance between the propeller disk and the trailing edge of the surface. Specifically, when the horizontal surface is in close proximity, the effect is positive, leading to an increase in generated thrust. On the other hand, in the case of the vertical surface, the effect is negative.
In conclusion, the push-pull propulsive solution presents exciting opportunities in the aircraft design field for the future, aligning with the growing resurgence of the propeller driven solution in a wide variety of implementations.

References

[1] Ira H. Abbott and Albert E. Von Doenhoff. *Theory of wing sections*. Dover Pubblications, INC., New York, 1949.

[2] K. Chinwicharnam and C. Thipyopas. Comparison of wing-propeller interaction in tractor and pusher configuration. *International Journal of Micro Air Vehicles*, 2016.

[3] Horne W. Clifton and Paul T. Soderman. Flow-field survey of an empennage wake interacting with a pusher propeller. *Technical memorandum NASA-TM-101003*, 1988.

[4] Weil Joseph and William C. Sleeman. Prediction of the effects of propeller operation on the static longitudinal stability of single-engine tractor monoplanes with flaps retracted. *Technical memorandum NACA-TR-941*, 1949.

[5] Jan Roskam. *Airplane Design*. Roskam Aviation and Engineering Corporation, 1985.

[6] Egbert Torenbeek. *Synthesis of Subsonic Airplane Design*. Springer-Science+Business Media, B.V., 1982.